Microstructure and Selected Properties of Cr₃C₂–NiCr Coatings Obtained by HVOF on Magnesium Alloy Substrates

Ewa Jonda [1],*, Leszek Łatka [2] and Wojciech Pakieła [1]

[1] Department of Engineering Materials and Biomaterials, Silesian University of
   Technology, Konarskiego St. 18a, 44-100 Gliwice, Poland; wojciech.pakiela@polsl.pl
[2] Department of Metal Forming, Welding and Metrology, Faculty of Mechanical Engineering, Wroclaw
   University of Science and Technology, Łukasiewicza St. 5, 50-371 Wroclaw, Poland; leszek.latka@pwr.edu.pl
* Correspondence: ewa.jonda@polsl.pl

check for
updates

Abstract: In present work the Cr_3C_2–NiCr coating was deposited on magnesium alloy substrate with high velocity oxygen fuel (HVOF) spraying. The microstructure of the samples has been characterized by means of electron microscopy, SEM and phase composition analysis carried out. The porosity of coatings has been also estimated. Finally, tests of selected mechanical properties, such as instrumented indentation, abrasive erosion have been performed. The results of the investigations confirmed that dense, homogeneous and well-adhered Cr_3C_2–NiCr cermet coating is possible to obtain onto the magnesium AZ31 alloy substrate. Moreover, the coatings exhibit high resistance to erosion.

Keywords: Cr_3C_2–NiCr cermet powder; HVOF spraying; magnesium AZ31 alloy; microstructure; instrumented indentation; erosion resistance

1. Introduction

For several years, magnesium alloys have been the subject of research in numerous scientific and research centers, as well as among industry producers, including automotive, machine construction, shipbuilding, aviation, chemical, energy, electronic and textile industries. Their low density (1.5–1.8 g/cm^3), the best among all currently known construction materials and high strength in relation to low weight, make these alloys able to be seen as the material of the future. However, low resistance to corrosion, erosion and abrasive wear can adversely affect and limit their widespread use [1–6]. The solution of this problem is to create protective layers, among others coatings applied by thermal spraying methods, which are used to extend the durability and life of machine parts, both new and remanufactured. Depending on the type of heat source used to melt the coating material, spraying can be distinguished: flame (low and high velocity), detonation, arc and plasma. The feedstock material could have a form of powder or wire. The most commonly used methods among above mentioned ones are the high velocity oxygen fuel (HVOF) and atmospheric plasma spraying (APS). The HVOF method allows the production of coatings with special properties, among others: low oxidation, very low porosity and high adhesion strength. Important advantage of this method is manufacturing coatings, which exhibit high abrasion resistance, protection against high temperature, erosion and corrosion. The wide variety of the feeding materials chemical composition makes it possible to produce coatings with dedicated properties for specific applications [7–10].

In the HVOF (high velocity oxygen fuel) process, molten or partially molten material particles are sprayed onto the substrate surface with a high-speed, high-temperature gas stream. The coating material is heated and accelerated with a gas stream jet, and then hits the surface of the deposited element. In this process, the gas stream is produced by mixing and igniting oxygen and fuel (gaseous or

liquid) in the combustion chamber, ensuring a rapid flow of gas under high pressure through the nozzle. The velocity of the gas stream that lifts the particles is supersonic. Particles of the coating material are introduced into the stream, heated and directed to the surface of the element. The mixture of oxygen and fuel creates high pressure in the combustion chamber, and then passing through the expanded Laval nozzle forms a shock wave. Gases that explode inside the shockwave melt the powder particles and transport it towards the substrate on which the coating is formed, see Figure 1 [11–15].
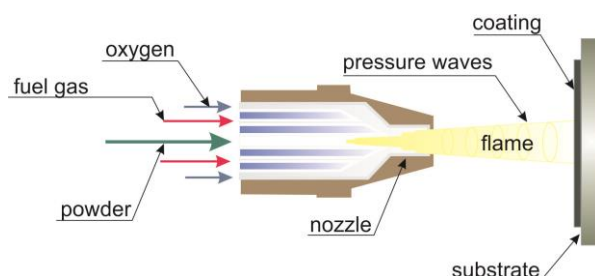

Figure 1. Scheme of the high velocity oxygen fuel (HVOF) spraying process, adapted from [8].

In the spraying process, the substrate material does not melt, and the sprayed coating is attached to the substrate mechanically, with adhesion or, in special cases, the connection is of metallurgical nature. Particles of material falling on the sprayed surface in a semi-plastic state are flattened and, adhering to each other in the form of successive layers, form a continuous coating. (Figure 2, scheme of the coating formation) [16–19].
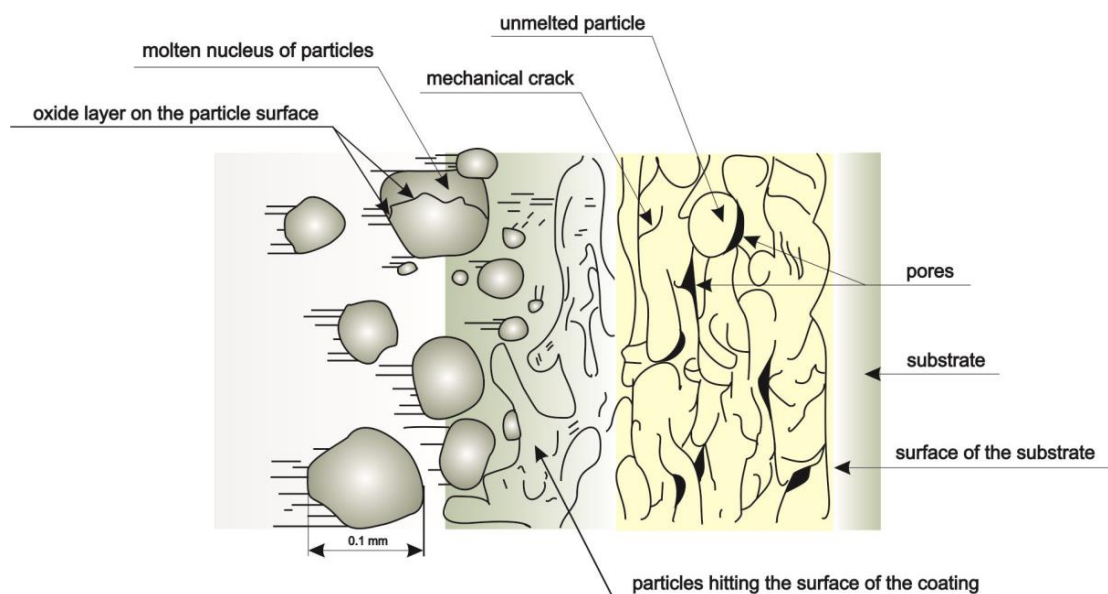

Figure 2. Scheme of the coating formation, adapted from [20].

The analysis of current research results in the field of coating production by means of supersonic flame spraying (HVOF) includes spraying, among others on alloy structural steels, non-alloy qualitative steels for thermal improvement, stainless and on nickel alloys, while the use of light construction materials as foundations in the form of magnesium alloys with low resistance to tribological factors has not been thoroughly studied and discussed so far.

Review of the presented results of experimental works indicates that in the field of development of modern techniques for improving or restoring the properties of the surface of an element by supersonic spraying, there are few studies on research works on the production of the abovementioned coatings on magnesium alloys [21–25].

In spite of plenty of research, there is still not enough information about the microstructure and properties of the Cr_3C_2–NiCr coatings obtained by HVOF on magnesium alloy substrates. This manuscript is going to be an attempt to fill this gap as a current topic, both from a scientific and application point of view.

In this publication, the authors focused on preliminary studies, which aim was check the possibility of manufacturing cermet coating using HVOF method onto AZ31 magnesium alloy. Additionally, these coatings should be characterized by good adhesion, low porosity and proper tribological properties. Therefore, the article presents and discusses the results only for one Cr_3C_2–NiCr coating obtained with initially optimized parameters by CERTECH Company, Wilamowice, Poland. In future research, authors will continue the optimization process for this powder in order to improve functional properties of obtained coatings.

2. Materials and Methods

2.1. Coatings Deposition

AZ31 magnesium alloy was selected as a substrate material, with the chemical composition: (elements, in wt %) Mn—0.17, Zn—1; Al—3, Ca—0.04, Cu—0.05 and Mg—balance, with 5 mm in the thickness (Institute of Non-Ferrous Metals in Gliwice, Skawina, Poland) [26]. The particle size of commercially available powder Cr_3C_2–25% wt. NiCr (Amperit 588.059) was in the range of 30 + 5 μm and supplied by Höganäs. The chemical composition of the feedstock powder, which was used in coatings manufacturing process is (elements, in wt %): Cr: 66–73, C: 9–11, Fe: <0.5, Ni: 15–22 and O: <0.6 [27].

The surface of samples was prepared by sandblasting with corundum to get a surface roughness in the range of Ra equal to 17 μm and ultrasonic treated to achieve god adhesion between coating and the substrate. C-CJS spray system Thermico (CERTECH Company, Wilamowice, Poland) was used to prepare coating. Kerosene and oxygen were used as the fuel gases, respectively, whereas nitrogen was used as the carrier gas. The maximum flame temperature with in the hottest point was about 3520 K, whereas the substrate surface temperature, including spray distance (280 mm) did not exceed 600 K. The spraying parameters are listed in Table 1.

Table 1. Process parameters of HVOF coating.

Coating Process	Cr_3C_2–NiCr
Kerosene flow rate, l/min	40
Oxygen flow rate, l/min	35
Nitrogen flow rate, l/min	10
Powder feed rate, g/min	25
Spray distance, mm	280

2.2. Coatings Characterization

2.2.1. The Microstructure

Microstructural investigations were carried out by means of scanning electron microscopy, SEM (Supra 35, Zeiss, Oberkochen, Germany) using secondary electron and backscattered detectors (TRIDENT XM4, Edax, 91 McKee DRIVE, Mahwah, NJ, USA). The chemical composition was analyzed by EDS (energy dispersive X-ray spectroscopy, Supra 35, Zeiss, Oberkochen, Germany). In order to determine the phase composition of the Cr_3C_2–NiCr coating, X-ray diffraction, XRD, tests were carried out. XRD investigations of sprayed coatings were done by an X-ray diffractometer X'Pert Pro MPD by Panalytical (Almelo, the Netherlands) apparatus with a copper anode lamp ($\lambda K\alpha = 0.154$ nm; Panalytical, Almelo, the Netherlands) as well as a PIXcel 3D detector (Panalytical, Almelo, the Netherlands) on the diffracted beam axis. The diffraction lines were recorded in the Bragg–Brentano geometry

in the angular scope of 15°–90°, with the step of 0.03° and the step time of 0.8 s. The analysis of the obtained diffraction patterns was made in the Panalytical High Score Plus software (Version 3.0e, Panalytical, Almelo, the Netherlands), containing a dedicated flat-file base of PAN-ICSD phase identification. The coating's surfaces observation was carried out with digital optical microscope Keyence VHX-5000 (Keyence International, Mechelen, Belgium). The surface morphology of the sprayed coating was examined using an atomic force microscope (AFM; XE-100 Park Systems Corp, Suwon, Korea).

2.2.2. Surface Topography, Porosity and Roughness

Measurements of surface topography were carried out under ambient conditions and with the use of a commercial scanning probe. The AFM topographic images were analyzed with the use of a dedicated XEI program (Version of XEI program-1.08, Park Systems Corp., Suwon, Korea). Using AFM microscopy (100 Park System, Park Systems Corp., Suwon, Korea), Ra (arithmetic mean of ordinates of the roughness profile) and Rz (maximum height of the roughness profile) roughness parameters were made. The sandblasting was used in order to increase the surface roughness, which is necessary to improve the coatings adhesion strength to the substrate. Image analysis with free software ImageJ (version 1-50) was used to determine the porosity level. The measurements were made according to the ASTM E2109-01 standard [28]. The porosity was assessed as an average from 20 images at 1000× magnification.

2.2.3. Mechanical Properties

The testing of mechanical properties was started by measurements of coatings adhesion strength. The bond-strength was determined by a well-known pull-off test and was carried out by a dedicated Elcometer 510 tester (Elcometer Instruments, Manchester, UK). A counter-part with the diameter of 10 mm was bonded to the coating using epoxy adhesive Distal Classic (Libella, Warsaw, Poland). Then, the continuous pressure of 0.1 MPa/s was applied to the test dolly. After the observations of coating surface and dolly surface, the failure mode was determined. The average value and standard deviation were calculated based on four measurements. Hardness of manufactured coatings was determined by an instrumented indentation test (IIT). Tests were carried out on an NHT^3 nanoindenter (Anton Paar, Graz, Austria), equipped with Berkovich indenter and were performed at room temperature on the cross sections in accordance with ISO 14577-4:2016 standard [29]. With this method, also an instrumented Young modulus of sprayed coating was determined, based on Oliver and Pharr methodology [30]. The details of the measurement procedure could be found in [31]. For hardness measurements, the value of the maximum load was equal to 500 mN, whereas for elastic modulus the range of maximum load was from 50 to 500 mN. In both cases the dwell time was equal to 15 s.

2.2.4. The Abrasion and Erosion Resistance

Tests of erosion resistance at room temperature were carried out at a specially constructed stand at the Welding Department of the Silesian University of Technology in Gliwice, according to the ASTM G76-04 standard [32]. The test used a nozzle tube with a diameter of 1.5 ± 0.075 mm located at a distance of 10 ± 1 mm from the sample, the angle of inclination of the nozzle in relation to the sample was 90°. The tests were carried out using Al_2O_3 abrasive with a grain diameter of 50 μm, particle feed rate of 2 ± 0.5 g/min and discharge velocity from the nozzle 70 m/s. The test duration was 5 min and was determined experimentally because at 10 min the erosion crater was deeper than 1 mm. In order to obtain reliable results, 10 tests were carried out with given parameters. Due to the very small weight losses bordering the measurement error, the erosion crater profiles were measured (digital optical microscope Keyence VHX-5000) and observed by the scanning electron microscope (SEM, Supra 35, Zeiss, Oberkochen, Germany). In addition to the erosion resistance tests, abrasion resistance tests were also performed. The abrasion resistance tests were carried out using the "pin-on-disc" method in accordance to the ASTM G99 standard [33]. The ZrO_2 (zirconium oxide) ball with a diameter of

6 mm was used as a counter-body. The tests were carried out at room temperature, with the following parameters: load—5 N, linear speed—20 cm/s and distance—500 m. During the test, the friction coefficient was measured. To determine the mechanism of the wear the topography was analyzed using an SEM and the wear track dimensions after tests were measured by a Sutronic 25-Taylor Hobson profilometer (Taylor Hobson Ltd., Leicester, England).

3. Results

3.1. The Microstructure

The structure observation in a scanning electron microscope was made in BSD (backscattered electrons) and SE (secondary electrons) mode. In the area of the layer did not disclose cracks or voids. The porosity level of the coating was equal to 2% ± 0.3% (Figure 3a,b). The occurrence of cracks and voids could result in reduced durability of the coating, as well as, crack propagation and finally delamination [34]. SEM micrographs of the coating have indicated unmelted carbide particles (dark areas on the Figure 3b) in the metallic (Ni–Cr) matrix. Size of the carbides in the layer did not exceed 3 μm. In addition, their shape (rounded edges) clearly indicates that they were melted during the HVOF process. Cr_3C_2 carbides were evenly distributed in the metal matrix (Figure 3b,c). Evenly distributed structure components, including carbides, significantly affect the strength of the coating. Sidhu et al. has come to similar conclusions. They combined the increase in hardness of the obtained coatings with a high volume of carbides that were well-dispersed in the matrix [35]. The shape and distribution of carbides in the matrix indicate correctly selected process parameters.
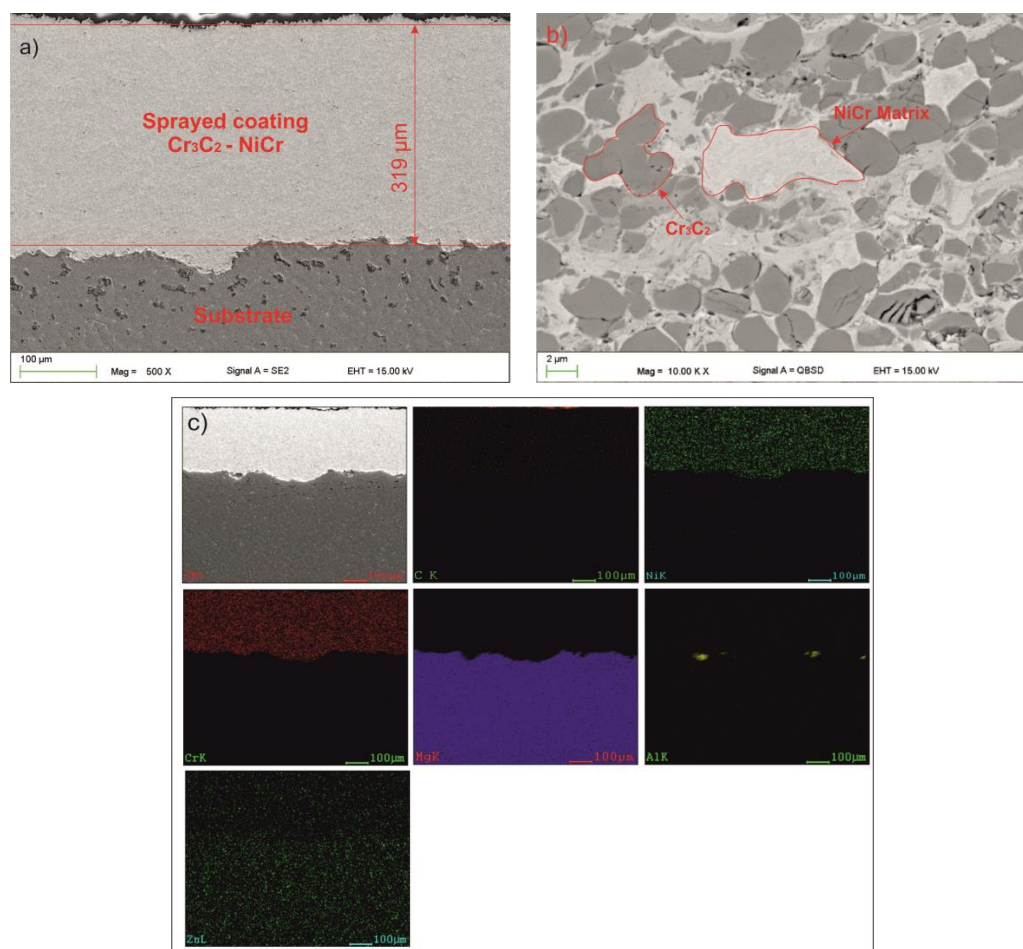

Figure 3. Structure of the coating (**a**) thickness; (**b**) central part of the layer and (**c**) elemental distribution maps of spraying elements in the analyzed area of the coating obtained during thermal spraying.

The average coating thickness ranged from 330 ± 15 μm. J.M. Guilemany et al. showed that the thickness of the thermal spray coating has a significant impact on the quality of the electrochemical barrier. They proved that the thickness of the coating should be at least 300 μm [36] (Figure 3a). Observations of the lower part of the layer showed that the connection is only adhesive and mechanical (Figure 4a). The layer adheres tightly to the substrate. The EDS analysis showed no evidence of a diffusion connection. Carbon in the chemical composition analysis should be treated only as a guide (Table 2).
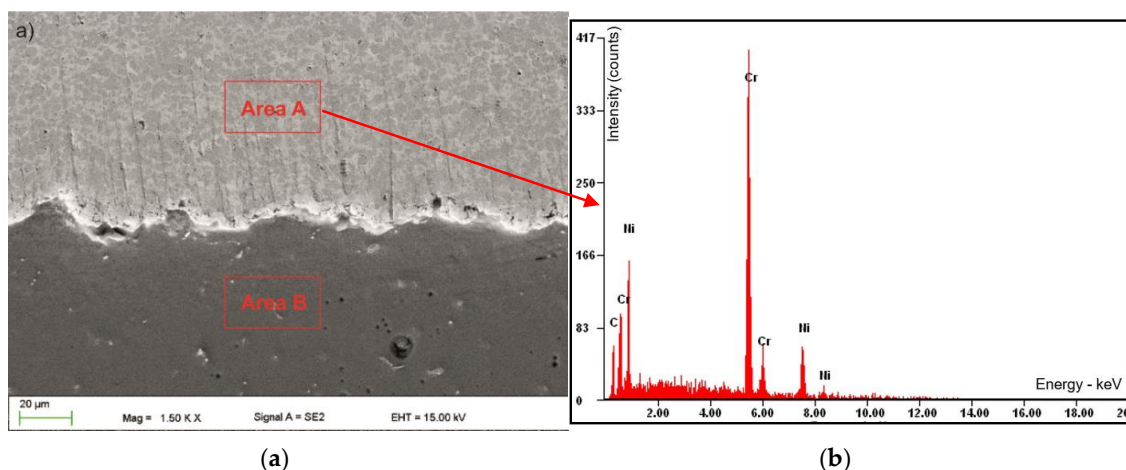

| (a) | (b) |

Figure 4. SEM cross-section images: area "A" coating and area "B" substrate (**a**) and the (**b**) EDS analysis of the coating.

Table 2. Chemical composition of layer and substrate from the Figure 5.

Area "A" from Figure 5			Area "B" from Figure 5		
Element	wt %	At%	Element	wt %	At%
C	11	35	Mg	94	95
Cr	60	45	Al	03	02
Ni	29	20	Zn	03	02
Matrix	Correction	ZAF *	Matrix	Correction	ZAF

* ZAF (Atomic number "Z", Absorption effect "A" and Fluorescence effect "F")-corrections used to EDS measurements to convert raw peak intensity into semi-quantitative concentrations corrected for inter-element matrix effects.
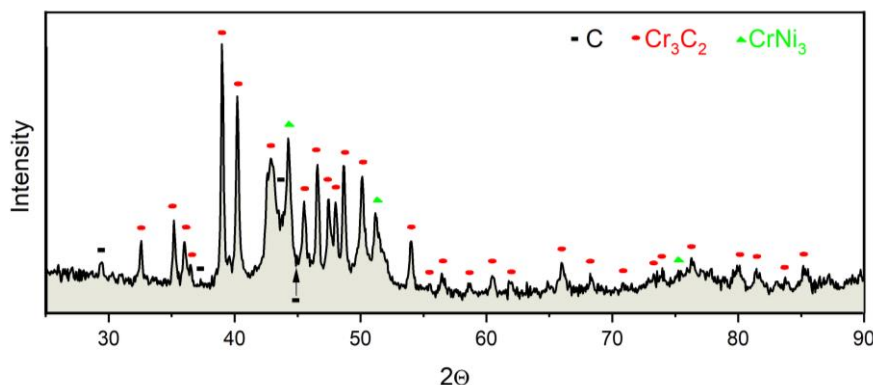

Figure 5. The phase composition of manufactured coating Cr_3C_2–NiCr deposited on AZ31 magnesium alloy.

In Figure 5 the X-ray diffraction pattern of manufactured coating is presented. It could be found two main phases: (i) an adhesive $CrNi_3$, which gives a high bonding strength as well as fracture toughness and (ii) a hard Cr_3C_2, which provides higher hardness and wear resistance. These phases

are also detected in [37]. In order to determine quantitative phase composition, the RIR (Reference Intensity Ratio) method has been used [38]. The results of these analyses are as follows: 65% of the Cr_3C_2 and 35% of the $CrNi_3$. These values are confirmed by [39,40].

3.2. The Topography and Roughness of Coating

The surface roughness parameters of the manufactured coating are collected in Table 3. The results were the average values from five measurements. Figure 6a,b shows the topography and (c) the roughness histogram over the entire surface of the coating. Similar values of the roughness parameters were observed for a medium carbon steel equivalent AISI4043 thermally sprayed WC–Co–Cr by HVOF [41] and also for part of the worn shafts of THM gas turbine engines with coatings of Cr_3C_2–25%NiCr and WC–12%Co powders carried out by thermal spray with supersonic flame (HVOF) [42]. The adhesive strength of HVOF Cr_3C_2–NiCr coating was from 42 to 44 MPa. The similar results (25–40 MPa) are shown by Wang et al. for WC–Co coating sprayed by HVOF on mild steel [43].

Table 3. The average surface roughness of the coating in the as-sprayed condition.

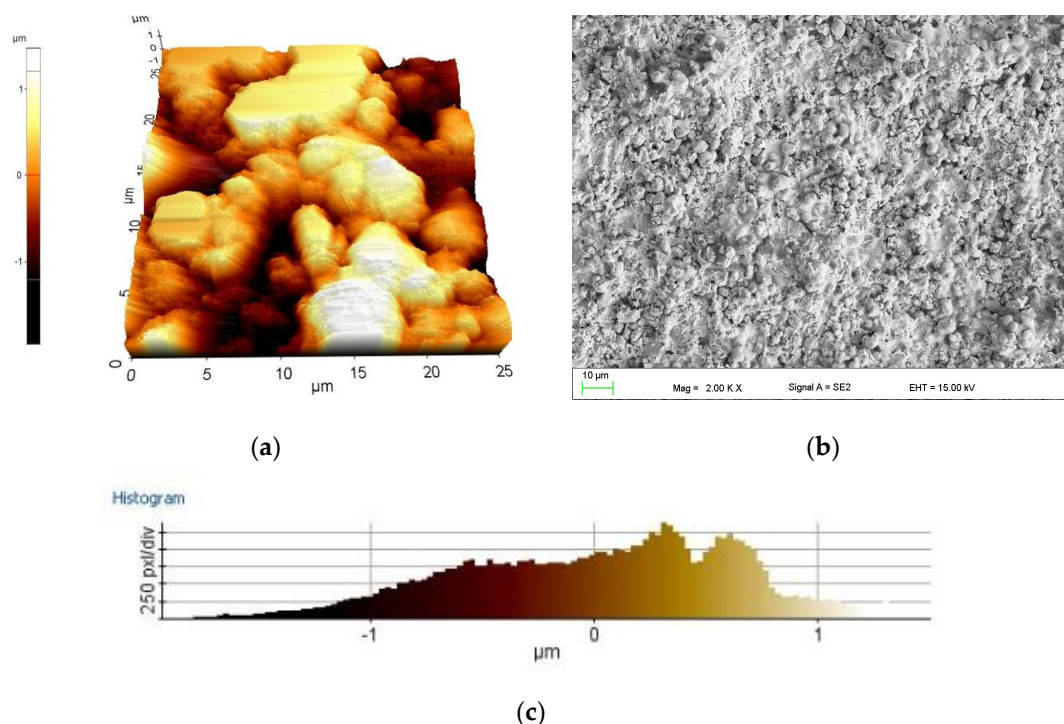| Roughness Parameter	Ra (Arithmetic Mean of Ordinates of the Roughness Profile)	Rz (Maximum Height of the Roughness Profile)
Surface roughness values, μm	1.368	8.813
Standard deviation	0.126	0.619

(a)

(b)

(c)

Figure 6. Topography of the thermally sprayed coating surface AFM (**a**) and SEM (**b**); roughness histogram over the entire surface of the coating (**c**).

3.3. Wear Resistance

Manufactured coating has good wear resistance as shown by the dry sliding wear test. The wear rate of investigated coatings was equal to $13.88 \pm 3.11 \times 10^{-6}$ mm^3/(N·m) and friction coefficient was equal to 0.6 ± 0.03. The typical wear trace is given in Figure 7. More details could be found in [44].
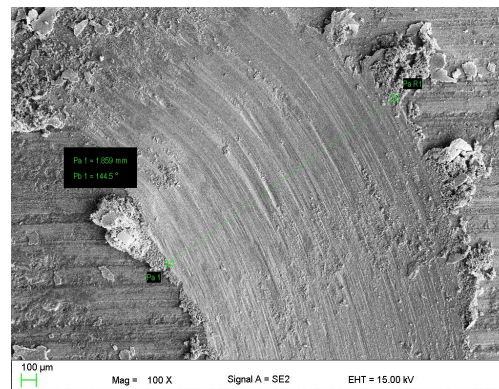
Figure 7. Wear tracks of Cr_3C_2–NiCr coatings, magnification 100×.

3.4. The Instrumented Indentation

The instrumented indentation tests have been carried out in order to determine microhardness and elastic modulus. In the case of hardness, the estimated value was equal to 8.7 ± 0.5 GPa and it was an average of 10 measurements. As it can be seen, the standard deviation value was quite small, which indicates low porosity and a homogenous structure (which is observed in Figure 6). Similar values for Cr_3C_2–NiCr coatings could be found in [37,45–47].

As it was mentioned above, from the unloading part of the indentation curve it is possible to determine the elastic modulus. For this purpose 10 indentation curves with the maximum load in range from 50 to 500 mN (with a step equal to 50 mN) were analyzed. The obtain value of the instrumented elastic modulus was equal to 224 GPa. This value was about 60% of the Young modulus for bulk material [48]. In comparison with another result in literature, the obtained value was similar. Slight differences could result in a different structure (mainly the porosity level) and details of the phase composition, which is a derivative of the process parameters [49,50].

3.5. The Erosion Resistance

The results of erosion test confirmed, that application of Cr_3C_2–NiCr composite coating strongly improves resistance against eroded particles. The erosion craters on the surfaces of the pure magnesium alloy substrate and covered by composite coating are presented in Figure 8. As it could be seen, the reduction of the erosion crater area was almost 25% for the coated surface.
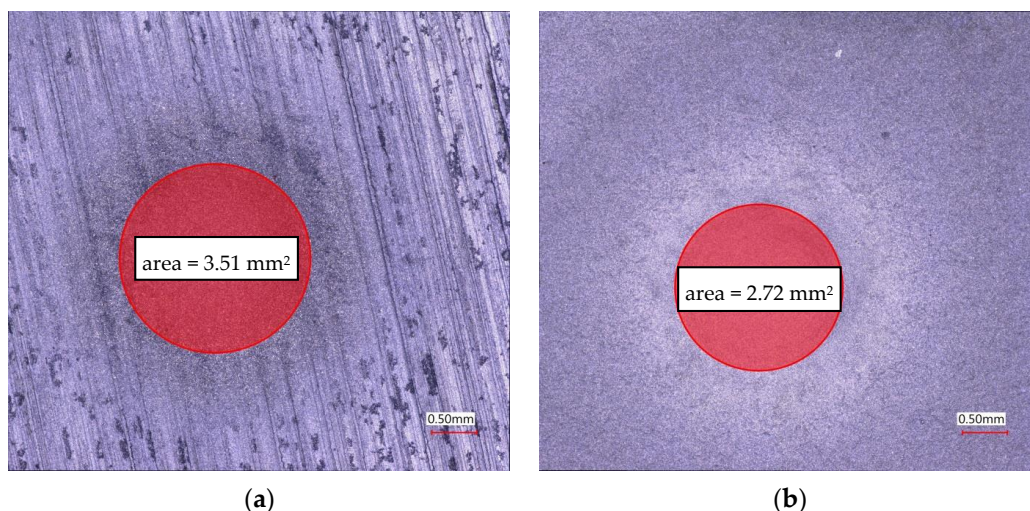

(**a**)   (**b**)

Figure 8. The comparison of the erosion craters of: (**a**) magnesium substrate and (**b**) composite coating.

Moreover, the virtual cross section made in Keyence VHX-5000 software allows one to estimate the crater depth. The measurement carried out in two perpendicular directions. The view of typical virtual cross section is presented in Figure 9. Detailed values of crater depth for both samples are collected in Table 4.
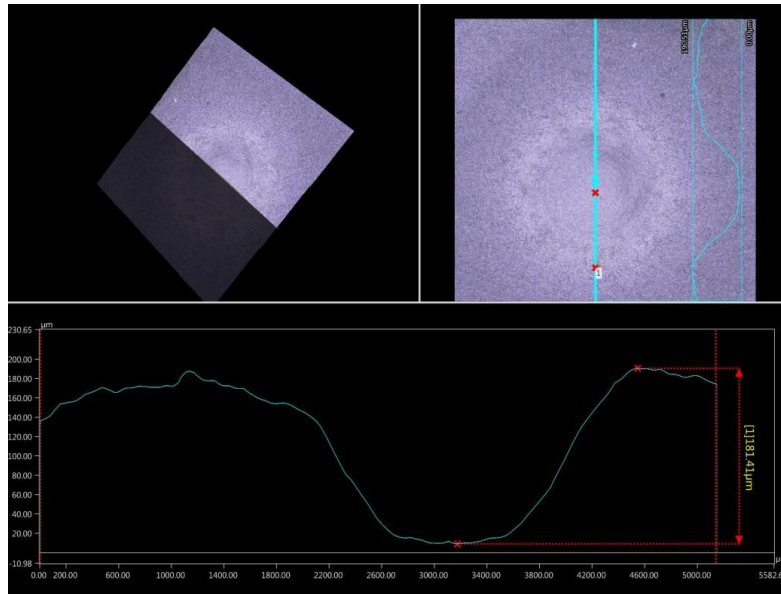

Figure 9. The virtual cross section of the crater of coated sample and its depth.

Table 4. The comparison of the crater depth for the uncoated and coated sample.

Direction of Virtual Cross Section	Horizontal	Vertical	Standard Deviation	
			Horizontal	Vertical
Uncoated AZ31 magnesium alloy	286.39 μm	249.88 μm	28.53	24.21
Coated AZ31 magnesium alloy	204.32 μm	181.41 μm	16.36	15.34

The calculated relative weight loss was equal to $0.054\% \pm 0.005\%$ and $0.013\% \pm 0.001\%$ for the uncoated and coated sample, respectively. The value for Cr_3C_2–NiCr coating was similar to that obtained by researchers in [51]. The typical surface of the coating after erosion is presented in Figure 10.

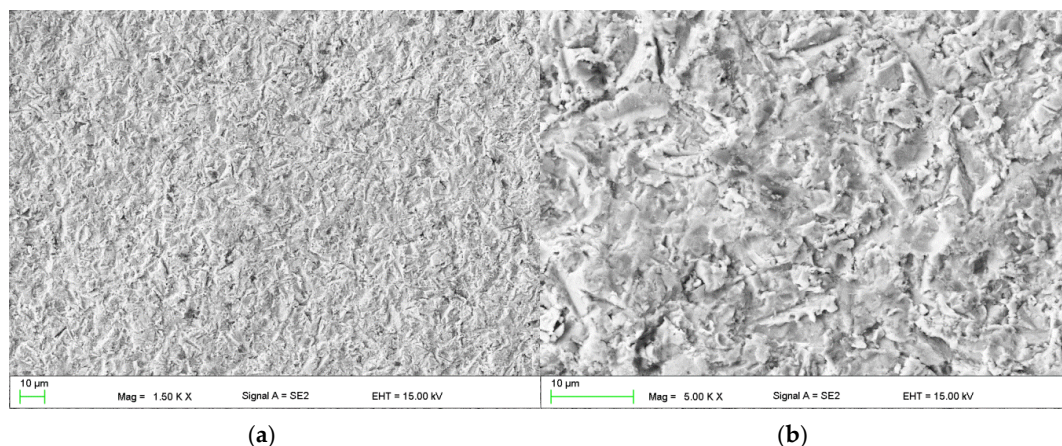(a)   (b)

Figure 10. Coatings surface after erosion test: (**a**) lower magnification (1500×) and (**b**) higher magnification (5000×).

The observation of eroded surface revealed the existing of the cracks, which were initiated in the weak cohesion areas and then propagated along the interfaces between the lamellae. Additionally,

the ploughing was visible [51]. The cracks exhibited a brittle type, despite the presence of ductile NiCr matrix. The occurred erosion mechanism is similar to the one observed and described by Matthews et al. [39].

4. Conclusions

Based on the tests carried out on the Cr_3C_2–NiCr coating deposited on the AZ31 magnesium alloy substrate with high velocity oxygen fuel (HVOF) spraying, the following conclusions could be made:

1. In the area of the coating did not disclose cracks or voids. The standard deviation value was quite small, which indicates on low porosity and homogenous structure (the porosity of the coating was around 2%). SEM micrographs of the coating have indicated unmelted carbide particles in metallic (Ni–Cr) matrix. Cr_3C_2 carbides were evenly distributed in the metal matrix. In the sprayed coatings are two main phases, namely Cr_3C_2 and $CrNi_3$.
2. The average coating thickness ranged from 330 ± 15 μm and the coating adhered tightly to the substrate. EDS analysis showed no evidence of a diffusion connection.
3. The roughness of the sprayed coating was greater than the roughness of the AZ31 magnesium alloy substrate (Ra = 0.31–0.4 μm) and the adhesive strength of coating was from 42 to 44 MPa.
4. Manufactured coating had good wear resistance and the dominant mechanism of wear was a classic adhesive one.
5. Application of the Cr_3C_2–NiCr composite coating strongly improve resistance against eroded particles. The calculated relative weight loss was equal to 0.054% and 0.013% for uncoated and coated sample, respectively.

References

1. Yang, X.; Liu, J.; Wang, Z.; Lin, X.; Liu, F.; Huang, W.; Liang, E. Microstructure and mechanical properties of wire and arc additive manufactured AZ31 magnesium alloy using cold metal transfer process. *Mater. Sci. Eng. A* **2020**, *774*, 138942. [CrossRef]
2. Mazaheri, Y.; Mahdi, M.; Akbar, J.; Amir, H.; Jahani, R. Tribological behavior of AZ31/ZrO$_2$ surface nanocomposites developed by friction stir processing. *Tribol. Int.* **2020**, *143*, 1–4. [CrossRef]
3. Yang, X.; Feng, W.-Y.; Li, W.; Dong, X.-R.; Xu, Y.-X.; Chu, Q.; Yao, S.-T. Microstructure and properties of probeless friction stir spot welding of AZ31 magnesium alloy joints. *Trans. Nonferrous Met. Soc. China* **2019**, *29*, 2300–2309. [CrossRef]
4. Fouad, Y.; El Batanouny, M. Effect of surface treatment on wear behavior of magnesium alloy AZ31. *Alex. Eng. J.* **2011**, *50*, 19–22. [CrossRef]
5. Taltavull, C.; Lopez, A.J.; Torres, B.; Atrens, A.; Rams, J. Optimization of the high velocity oxygen fuel (HVOF) parameters to produce effective corrosion control coatings on AZ91 magnesium alloy. *Mater. Corros.* **2015**, *66*, 423–432. [CrossRef]
6. Song, G.; Xu, Z. The surface, microstructure and corrosion of magnesium alloy AZ31 sheet. *Electrochim. Acta* **2010**, *55*, 4148–4161. [CrossRef]
7. Somasundaram, B.C.; Jegadeeswaran, N.; Mamatha, M.P. Wear behavior of HVOF sprayed WC–Co/NiCrAlYSi (35–65%) and WC–Co/NiCrAlYSi (80%–20%) coatings on turbine SS316 steel. *Mater. Today Proc.* **2020**, *20*, 103–107. [CrossRef]
8. Yadaw, R.C.; Singh, S.K.; Chattopadhyaya, S. Tribological behavior of thin film coating-a review. *Int. J. Eng. Technol.* **2018**, *7*, 1656–1663. [CrossRef]

9.　Formanek, B.; Szymański, K.; Kuczowitz, B. Corrosion and abrasion resistant coatings obtained by thermal spraying methods. *Prot. Against Corros.* **2010**, *53*, 164–168.

10.　Hejwowski, T. *Modern Heat-Applied Coatings Resistant to Wear Abrasive and Erosive 2013 Lublin*; Biblioteka Cyfrowa Politechniki Lubelskiej: Lublin, Poland; Available online: http://bc.pollub.pl/dlibra/publication/5141/edition/4059?language=pl(accessed on 15 June 2020)ISBN 978-83-63569-56-3.

11.　Radziszewski, A. Thermal spray coatings from non-ferrous metals and their alloys (Industrial applications). *Weld. Technol. Rev.* **2014**, *2*, 33–39.

12.　Robertson, A.L.; White, K.W. Microscale fracture mechanisms of a Cr_3C_2–NiCr HVOF coating. *Mater. Sci. Eng. A* **2017**, *688*, 62–69. [CrossRef]

13.　Shabana; Sarcar, M.; Suman, K.; Kamaluddin, S. Tribological and Corrosion behavior of HVOF Sprayed WC–Co, NiCrBSi and Cr3C2-NiCr Coatings and analysis using Design of Experiments. In *Proceedings of the Materials Today: Proceedings*; Elsevier BV: Amsterdam, The Netherlands, 2015; Volume 2, pp. 2654–2665.

14.　Otsubo, F.; Era, H.; Uchida, T.; Kishitake, K. Properties of Cr_3C_2–NiCr Cermet Coating Sprayed by High Power Plasma and High Velocity Oxy–Fuel. *J. Therm. Spray Technol.* **2000**, *9*, 499–504. [CrossRef]

15.　Liu, Q.; Bai, Y.; Wang, H.; Ma, G.; Liu, M.; Chu, C.; Sun, Y.; Fan, W.; Ding, F.; Zhao, B.; et al. Microstructural evolution of carbides and its effect on tribological properties of SAPS or HVOF sprayed NiCr–Cr_3C_2 coatings. *J. Alloy. Compd.* **2019**, *803*, 730–741. [CrossRef]

16.　Janka, L. Thermally Sprayed Cr_3C_2–NiCr Coatings -Improving the Abrasion Resistance. Ph.D. Thesis, Tampere University of Technology, Tampere, Finland, 2018. Available online: http://www.tut.fi/tutcris (accessed on 15 June 2020).

17.　Zdravecka, E.; Suchanek, J.; Tkacova, J.; Trpcevska, J.; Brinkienė, K. Investigation of wear resistance of high velocity oxy-fuel sprayed WC–Co and Cr_3C_2–NiCr coatings. *Mechanika* **2010**, *4*, 75–79.

18.　Ang, A.S.M.; Howse, H.; Wade, S.; Berndt, C. Development of Processing Windows for HVOF Carbide-Based Coatings. *J. Therm. Spray Technol.* **2015**, *25*, 28–35. [CrossRef]

19.　Ben Hamu, G.; Eliezer, D.; Wagner, L. The relation between severe plastic deformation microstructure and corrosion behavior of AZ31 magnesium alloy. *J. Alloy. Compd.* **2009**, *468*, 222–229. [CrossRef]

20.　Pnc S.C. Natryskiwanie Cieplne Powłok. Available online: https://www.pnc.pl/natryskiwanie-cieplne/podstawy-procesu-metalizacji-natryskowej.html (accessed on 15 June 2020).

21.　Buchtík, M.; Másilko, J.; Vyklický, O.; Filipenský, J.; Wasserbauer, J.; Ptácek, P. Microstructural characterization and wear behavior of WC-COCr coating on AZ91 magnesium alloy. In Proceedings of the METAL 2019—28th International Conference on Metallurgy and Materials, Conference Proceedings: Hotel Voronez I, Brno, Czech Republic, 22–24 May 2019; pp. 922–927.

22.　Yıldız, F. Tribological Properties of WC-12Co Coating on AZ91 Magnesium Alloy Fabricated by High Velocity Oxy-Fuel Spray. *High Temp. Mater. Process.* **2014**, *33*, 41. [CrossRef]

23.　Parco, M.; Zhao, L.; Zwick, J.; Bobzin, K.; Lugscheider, E. Investigation of HVOF spraying on magnesium alloys. *Surf. Coat. Technol.* **2006**, *201*, 3269–3274. [CrossRef]

24.　Lopez, A.J.; Torres, B.; Taltavull, C.; Rams, J. Influence of high velocity oxygen-fuel spraying parameters on the wear resistance of Al–SiC composite coatings deposited on ZE41A magnesium alloy. *Mater. Des.* **2013**, *43*, 144–152. [CrossRef]

25.　Weisheit, A.; Lenz UMordike, B.L. Thermal spraying on magnesium alloys to improve the corrosion and wear resistance. *Metall* **1997**, *51*, 470–474.

26.　Yang, Z.; Li, J.; Zhang, J.; Lorimer, G.; Robson, J. Review on Research and Development of Magnesium Alloys. *Acta Met. Sin. (English Lett.)* **2008**, *21*, 313–328. [CrossRef]

27.　Höganäs.com Powder technologies. Surface coating. Available online: https://www.hoganas.com/globalassets/download-media/stc/pd-4057.pdf (accessed on 15 June 2020).

28.　*Standard Test Methods for Determining Area Percentage Porosity in Thermal Sprayed Coatings*; ASTM International: West Conshohocken, PA, USA, 2014.

29.　ISO, 14577-4:2016. *Metallic Materials-Instrumented Indentation Test for Hardness and Materials Parameters-Part 4: Test Method for Metallic and Non-Metallic Coatings*; International Organization for Standardization: Winterthur, Switzerland, 2016.

30.　Oliver, W.; Pharr, G. An improved technique for determining hardness and elastic modulus using load and displacement sensing indentation experiments. *J. Mater. Res.* **1992**, *7*, 1564–1583. [CrossRef]

31. Łatka, L.; Chicot, D.; Cattini, A.; Pawlowski, L.; Ambroziak, A. Modeling of elastic modulus and hardness determination by indentation of porous yttria stabilized zirconia coatings. *Surf. Coat. Technol.* **2013**, *220*, 131–139. [CrossRef]

32. *Standard Test Method for Conducting Erosion Tests by Solid Particle Impingement Using Gas Jets*; ASTM International: West Conshohocken, PA, USA, 2004.

33. *Standard Test Method for Wear Testing with a Pin-on-Disk Apparatus*; ASTM International: West Conshohocken, PA, USA,, 2017.

34. Espallargas, N.; Berget, J.; Guilemany, J.; Benedetti, A.V.; Suegama, P. Cr$_3$C$_2$–NiCr and WC–Ni thermal spray coatings as alternatives to hard chromium for erosion–corrosion resistance. *Surf. Coat. Technol.* **2008**, *202*, 1405–1417. [CrossRef]

35. Sidhu, H.S.; Sidhu, B.S.; Prakash, S. Mechanical and microstructural properties of HVOF sprayed WC–Co and Cr$_3$C$_2$–NiCr coatings on the boiler tube steels using LPG as the fuel gas. *J. Mater. Process. Technol.* **2006**, *171*, 77–82. [CrossRef]

36. Guilemany, J.; González, J.F.; Delgado, J.; Benedetti, A.V.; Climent, F. Effects of thickness coating on the electrochemical behaviour of thermal spray Cr$_3$C$_2$–NiCr coatings. *Surf. Coat. Technol.* **2002**, *153*, 107–113. [CrossRef]

37. Lin, L.; Li, G.; Wang, H.; Kang, J.-J.; Xu, Z.-L.; Wang, H.-J. Structure and wear behavior of NiCr–Cr$_3$C$_2$ coatings sprayed by supersonic plasma spraying and high velocity oxy-fuel technologies. *Appl. Surf. Sci.* **2015**, *356*, 383–390. [CrossRef]

38. Prevéy, P.S. X-Ray Diffraction Characterization of Crystallinity and Phase Composition in Plasma-Sprayed Hydroxyapatite Coatings. *J. Therm. Spray Technol.* **2000**, *9*, 369–376. [CrossRef]

39. Matthews, S.; James, B.; Hyland, M. The role of microstructure in the mechanism of high velocity erosion of Cr$_3$C$_2$–NiCr thermal spray coatings: Part 1–As-sprayed coatings. *Surf. Coat. Technol.* **2009**, *203*, 1086–1093. [CrossRef]

40. Karaoglanli, A.C.; Oge, M.; Doleker, K.M.; Hotamis, M. Comparison of tribological properties of HVOF sprayed coatings with different composition. *Surf. Coat. Technol.* **2017**, *318*, 299–308. [CrossRef]

41. Murthy, J.K.N.; Rao, D.S.; Venkataraman, B. Effect of grinding on the erosion behavior of a WC–Co–Cr coating deposited by HVOF and detonation gun spray processes. *Wear* **2001**, *249*, 592–600. [CrossRef]

42. Sahraoui, T.; Fenineche, N.-E.; Montavon, G.; Coddet, C. Structure and wear behaviour of HVOF sprayed Cr$_3$C$_2$–NiCr and WC–Co coatings. *Mater. And Des.* **2003**, *24*, 309–313. [CrossRef]

43. Wang, Y.-Y.; Li, C.-J.; Ohmori, A. Influence of substrate roughness on the bonding mechanisms of high velocity oxy-fuel sprayed coatings. *Thin Solid Films* **2005**, *485*, 141–147. [CrossRef]

44. Jonda, E.; Łatka, L.; Wiecław, G. Preliminary studies on HVOF sprayed coatings on the magnesium alloys. *Coatings* **2020**, *10*. in press.

45. Sidhu, H.S.; Sidhu, B.S.; Prakash, S. Wear characteristics of Cr$_3$C$_2$–NiCr and WC–Co coatings deposited by LPG fueled HVOF. *Tribol. Int.* **2010**, *43*, 887–890. [CrossRef]

46. Houdková, Š.; Česánek, Z.; Smazalová, E.; Lukáč, F. The High-Temperature Wear and Oxidation Behavior of CrC-Based HVOF Coatings. *J. Therm. Spray Technol.* **2017**, *27*, 179–195. [CrossRef]

47. Lengauer, W. Transition Metal Carbides, Nitrides and Caronitrides. In *Handbook of Ceramic Hard Materials*; Riedel, R., Ed.; Wiley-VCH: Weinheim, Germany, 2000.

48. Varis, T.; Suhonen, T.; Calonius, O.; Čuban, J.; Pietola, M. Optimization of HVOF Cr$_3$ C$_2$ NiCr coating for increased fatigue performance. *Surf. Coat. Technol.* **2016**, *305*, 123–131. [CrossRef]

49. Bobzin, K.; Zhao, L.; Öte, M.; Königstein, T.; Steeger, M. Impact wear of an HVOF-sprayed Cr$_3$C$_2$–NiCr coating. *Int. J. Refract. Met. Hard Mater.* **2018**, *70*, 191–196. [CrossRef]

50. Szymański, K.; Hernas, A.; Moskal, G.; Myalska, H. Thermally sprayed coatings resistant to erosion and corrosion for power plant boilers-A review. *Surf. Coat. Technol.* **2015**, *268*, 153–164. [CrossRef]

51. Ji, G.-C.; Li, C.-J.; Wang, Y.-Y.; Li, W. Erosion Performance of HVOF-Sprayed Cr$_3$C$_2$–NiCr Coatings. *J. Therm. Spray Technol.* **2007**, *16*, 557–565. [CrossRef]